Exploring Mechanism of Corrosion Inhibition of WE43 and AZ31 Alloys by Aqueous Molybdate in Hank's Solution by Multisine Impedimetric Monitoring

Maria A. Osipenko[a,b], Jakub Karczewski[a], Michał Dominów[a], Marta Prześniak-Welenc[a], Jacek Gurgul[c], Iryna I. Kurilo[b], Jacek Ryl[a,*], and Dzmitry S. Kharytonau[d,e*]

[a]Advanced Materials Center and Institute of Nanotechnology and Materials Engineering, Gdańsk University of Technology, 80-233 Gdańsk, Poland

[b]Department of Physical, Colloid and Analytical Chemistry, Belarusian State Technological University, Minsk 220006, Belarus

[c]Surface Nanostructures Group, Jerzy Haber Institute of Catalysis and Surface Chemistry, Polish Academy of Sciences, Krakow 30-239, Poland

[d]Electrochemistry and Corrosion Laboratory, Jerzy Haber Institute of Catalysis and Surface Chemistry, Polish Academy of Sciences, Krakow 30-239, Poland

[e]Nanostructures of Soft Matter Group, Jerzy Haber Institute of Catalysis and Surface Chemistry, Polish Academy of Sciences, Krakow 30-239, Poland

*Corresponding authors:

Jacek Ryl: jacek.ryl@pg.edu.pl; Advanced Materials Center and Institute of Nanotechnology and Materials Engineering, Gdańsk University of Technology, 80-233 Gdańsk, Poland

Dzmitry S. Kharytonau: dmitry.kharitonov@ikifp.edu.pl; Jerzy Haber Institute of Catalysis and Surface Chemistry, Polish Academy of Sciences. Tel. +48782037574

Abstract:

The concept of utilizing multisine dynamic electrochemical impedance spectroscopy and distribution of relaxation times analysis to monitor effectiveness of a model molybdate inhibitor for AZ31 and WE43 Mg alloys is proposed. The corrosion kinetics and instantaneous values of inhibition efficiency (*IE*) of molybdate at concentrations up to 150 mM were examined. The inhibitor provides inhibition in Hank's solution at concentrations starting from ca. 25 mM, with the *IE* of about 90%. These data together with results of the surface analysis allowed to propose the mechanism of the corrosion inhibition of AZ31 and WE43 Mg alloys by aqueous molybdate in Hank's solution.

Keywords: Magnesium alloy; Molybdate Inhibitor; Multisine electrochemical impedance spectroscopy; Inhibition Mechanism

Highlights

- Effectiveness of molybdate inhibitor in Hank's solution towards AZ31 and WE43 Mg alloys has been examined;
- Multisine impedance analysis confirmed its usefulness for examination of inhibitor performance;
- Inhibition effect is provided by a surface film of mixed Mo(V)/Mo(VI) species;
- A two-stage mechanism of corrosion inhibition of Mg alloys by aqueous molybdate has been proposed.

1. Introduction

Magnesium alloys combine light weight with favorable mechanical properties, biocompatibility, and osteoconductivity [1,2]. Commercially available Mg alloys, such as AZ31 and WE43 are widely examined as promising materials for biomedical applications [3]. In this role, they can be used as temporary implant materials, whose degradation with time allows to avoid additional surgeries, while their degradation products can be absorbed or discharged by the human body [4,5].

While the biosafety of Mg alloys has been confirmed in numerous studies [6–8], their practical application is still limited due to their fast degradation rate in physiological environments [9,10]. This causes preliminary loss of mechanical properties and decreases the healing rate of native bone tissue [11]. The corrosion behavior of Mg and its alloys in physiological media is widely reported in the literature [12–17]. One of the ways to efficient corrosion control is the implementation of soluble corrosion inhibitors [18]. Corrosion inhibitors can be used as an individual component of the corrosion protection scheme or in combination with other types of conventional surface treatments, for example, plasma electrolytic oxidation coating, or layered double hydroxide carriers [18–20]. Precipitation and passivation inhibitors can precipitate in the form of insoluble compounds similar to conversion coating, forming a surface protective layer [19]. The selection of effective biocompatible inhibitors can be considered a promising strategy to control the degradation profile of Mg alloys in physiological media.

In recent literature, the inhibition effect of inorganic oxyanions (molybdate, selenite, permanganate, vanadate, phosphate) in chloride-containing aqueous solutions has been discussed [21–25]. These inhibitors can form a surface protective layer, similar to conversion treatment [19,26]. However, there are no studies of such inhibitors reported in the literature in the biologically relevant media.

The typical examination of the corrosion performance of Mg alloys includes electrochemical (linear polarization and electrochemical impedance spectroscopy (EIS)) and unpolarized (weight loss, hydrogen evolution, pH monitoring) measurements. However, classical electrochemical methods, such as EIS and potentiodynamic polarization have important limitations in the case of Mg alloys corrosion. In their recent study Wang et al. [27] showed the importance of the system non-stationarity as one of the possible origins of inductive low-frequency EIS response. Moreover, in our recent study [28], we proposed a multisine dynamic impedance spectroscopy (DEIS) as a tool for monitoring non-stationary electrochemical process. We have shown that DEIS in galvanostatic mode coupled with the distribution of relaxation times (DRT) analysis can be effectively utilized for precise real-time monitoring of corrosion processes. Decomposition of the multisine DEIS signal allows obtaining instantaneous impedance spectra and avoiding ambiguities and artifacts associated with changes in the measured system and its impedance characteristics during the measurement in nonstationary conditions [29]. The DRT analysis allowed for an in-depth and precise localization of the number and the kinetics of the ongoing electrochemical processes.

Despite being an effective tool in the examination of the corrosion process, the DEIS can be also used to study the kinetics of corrosion inhibition by soluble inhibitors, which was shown for Al alloys [30–32]. Therefore, it is of interest to develop an approach for multisine DEIS impedimetric examination of the inhibitor performance for highly reactive Mg alloys. Moreover, the correlation of the inhibition mechanism with the DRT analysis can bring a better fundamental understanding of the action of a particular inhibitor.

In this study, sodium molybdate Na_2MoO_4 was selected as a model inhibitor to evaluate the capability of DEIS monitoring towards examination of the inhibition mechanisms for Mg alloys corrosion. In our previous works [21,22,33] we have showed that soluble molybdates are effective

corrosion inhibitors of Al and Mg alloys in NaCl solutions. The inhibitive action of molybdates is associated with the formation of surface Mo mixed-oxide protective layers [19,21,22,33]. Moreover, in aqueous NaCl solutions soluble molybdates showed inhibition performance which strongly depends on their concentration [21,22]. The best inhibitor performance was reached in the solutions containing 100–150 mM of the molybdate inhibitor. Therefore, the maximum inhibitor concentration examined in this study (150 mM) was selected based on our previous publications [21,22].

Recently, molybdenum has been extensively examined as a biocompatible biodegradable material for medical applications [34,35]. Degradation of metallic Mo proceeds through the formation of surface Mo(IV, V, and VI) oxides, which are later dissolved [36]. Molybdates are not toxic with a high predicted no-effect concentration PNEC of 12.7 mg/L in freshwater and 1.90 mg/L in marine environments [37]. The dietary allowance for Mo in the human body is 45 μg/day (0.64 μg/kg/day) for adults [38], while excessive Mo beyond the physiologically normal total values is renally excreted [39], which should allow for metabolic clearance of molybdate released from a degrading surface protective layers without tissue accumulation [40]. For these reasons, molybdates can be considered as a possible alternative for a permanent surface protective coatings of Mg alloys. However, such high concentrations of any inhibitor cannot be used in real biomedical applications. Therefore, the motivation of the present study is to develop a reliable approach for the *in vitro* evaluation of the inhibitor performance for Mg alloys rather than the commercial application of molybdates in biomedical materials.

This study aims to examine the usefulness of the combined multisine impedance and DRT analysis to study the kinetics of non-stationary, highly dynamic corrosion of Mg alloys upon its interaction with the corrosion inhibitor. These are important aspects in the provision of reliable maintenance of metallic materials. To do so, we have selected two different types of Mg alloys

Mg-Al-Mn (AZ31) and Mg-Y-RE (WE43), and sodium molybdates as the corrosion inhibitor with high effectiveness towards such types of Mg alloys [21,22]. A specific focus is paid to instantaneous impedimetric monitoring of corrosion processes depending on the concentration of an inhibitor and exposure time. A comparison of the obtained data with the results of the multisine impedimetric monitoring of the AZ31 and WE43 alloys in Hank's solution without the molybdate inhibitor allowed for the estimation of the inhibition efficiency. Additionally, scanning electron microscopy (SEM) and X-ray photoelectron spectroscopy (XPS) measurements were used to elucidate and discuss the mechanism of corrosion inhibition provided by aqueous molybdate in Hank's solution.

2. Experimental

2.1. Materials

Commercially available Mg alloys AZ31 and WE43 were purchased from Smiths High Performance (UK). The chemical composition of the alloys as provided by the supplier is (wt.%) i) AZ31: Al 3.0%, Zn 1.0%, Mn 0.3%, and Mg balance; ii) WE43: Nb 2.2%, Y 3.7%, Zr 0.5%, and Mg balance. The detailed examination of the microstructure of these alloys is provided in our previous contributions and is beyond the scope of the present study [21–23].

As-received alloys were cut to samples with sizes 20×20×3 mm^3 for electrochemical studies and 10×10×3 mm^3 for surface analysis. Before measurements samples were mechanically ground in 99.9% ethanol to avoid their rapid corrosion using emery papers up to P2500-grit without further polishing.

Corrosion monitoring was carried out in Hank's solution of the chemical composition (g/L): 8.0 NaCl, 0.4 KCl, 0.14 $CaCl_2$, 0.2 $MgSO_4 \cdot 7H_2O$, 0.1 $MgCl_2 \cdot 6H_2O$, 0.35 $Na_2HPO_4 \cdot 2H_2O$, 0.06 KH_2PO_4 and 0.35 $NaHCO_3$. All the chemicals were purchased from Merck Life Science and

ChemPur (Poland) and were of analytical reagent grade. As a source of molybdate ions, $Na_2MoO_4 \times 2H_2O$ (≥99.5) received from Chemsolute (Th. Geyer Polska, Poland), was used. The solutions containing molybdate ions were stored in closed flasks for at least 24 h under laboratory conditions (~20 ◦C) to ensure equilibration of Mo species.

2.2. DEIS measurements

The DEIS electrochemical impedance spectroscopy measurements were carried out in a three-electrode setup using a BioLogic SP300 potentiostat. The measurements were performed in the galvanostatic mode at $i_{DC} = 0$ to imitate the open circuit potential (OCP) conditions and assure that no external polarization due to the OCP change will occur during each impedance measurement. The multisinusoidal AC perturbation signal package was composed of elementary sine waves in a frequency range from 22000 Hz to 0.7 Hz with 10 points per decade of frequency. The sampling frequency was 128 kHz. The peak-to-peak amplitude of perturbation signal was chosen to assure that the response signal amplitude would not exceed 15 mV. The frequency interval was selected to ensure the applicability of the DRT analysis. DEIS measurements were performed with a set of PXIe-6124 measurement card (National Instruments, USA) for the generation of AC multisinusoidal perturbation signal and a PXIe-4464 measurement card (National Instruments, USA) for the acquisition of AC/DC response signal. Cards operated in PXI-1073 chassis. A detailed description of the used multisine DEIS technique is available elsewhere [29,41–43]. A saturated Ag/AgCl electrode was used as the reference electrode, a Pt mesh was used as the counter electrode, and magnesium alloys were used as the working electrode. The surface area of the working electrode was 0.6 cm^2. The total volume of the electrolyte was 60 mL. A heating immersion thermostat (Julabo, Germany) was used to maintain a constant temperature of the

corrosion medium at 37.0 ± 0.1°C. The fitting of the obtained impedance spectra was performed using fitting software based on the Nelder-Mead algorithm [44].

To investigate the mechanism of corrosion inhibition by aqueous molybdates, DEIS spectra were recorded according to the following procedure. First, DEIS spectra of the sample in Hank's solution without the inhibitor were recorded for 10 min. Next, Hank's solution containing sodium molybdate with a concentration of 600 mM was continuously injected into the examined system using a peristaltic pump (Baoding Lead Fluid), using a previously adapted approach [31,45]. The initial volume of the electrolyte was 45 mL and reached 60 mL after the inhibitor immersion. The flow rate was set up in a way to achieve the final concentration of 150 mM of the Na_2MoO_4 inhibitor in the electrochemical cell after 50 min (the total time of the measurement was 1 h). The time-concentration profiles of Na_2MoO_4 injection in Hank's solution (Fig. S1 in the supplementary information) were used to calculate the inhibition efficiency. To ensure the homogeneity of the solution, continuous stirring was applied in the case of the measurements with and without the inhibitor. The DRT analysis was proposed to obtain information regarding the charge transfer resistance and protective layer capacitance, due to the inability to adapt a single electric equivalent circuit (EEC) for a dynamically changing corrosive environment and a multitude of processes instantaneously affecting the charge transfer. This study was followed by a 12 h exposure of the Mg alloys in the aforementioned electrolyte to assess the reliability of the corrosion inhibition in time. For the pH monitoring, a Schott Titroline Easy titrator was used. To ensure reproducibility, all electrochemical measurements were at least duplicated. The results reported in this contribution show representative data of the one selected measurement procedure.

2.3. DRT analysis

DRT analysis was done with the use of DRTtools software [46] with additional automatization provided by an own-made Python script. Regularization parameter value 1E-7 was used. Resistance values of the processes were acquired by integration of a field under the curve with trapezoidal numerical integration method, also provided by created program.

2.4. Physicochemical and surface analysis techniques

The microstructure of the WE43 and AZ31 alloys after exposure to Hank's solution was studied using an FEI Quanta 250 FEG Scanning Electron Microscope (SEM) under the accelerating voltage of 20 kV. An Energy Dispersive X-Ray Spectroscopy (EDX) detector attached to the SEM was used to study the surface chemical composition.

High-resolution X-ray photoelectron spectroscopy (XPS) measurements were performed after corrosion experiments using an SES R4000 Gammadata Scienta hemispherical analyzer. The measurement was performed by a monochromatized AlKα (1486.6 eV) X-ray source with the anode operating at 12 kV and 15 mA. Before measurements samples were sorely rinsed with deionized water and dried in a flow of nitrogen. The survey scans were collected at pass energy of 200 eV (with 0.25 eV step) and high-resolution spectra were collected at pass energy of 100 eV (with 25 meV step). The spectra analysis was performed by CasaXPS 2.3.23 software after subtraction of the Shirley-type background and fitting the experimental curve with a combination of Gaussian and Lorentzian lines of variable proportions (70:30). All obtained spectra were charge-corrected to the adventitious carbon C 1s (285.0 eV).

3. Results and discussion

Application of the multisine DEIS measurement technique allowed for instantaneous and precise monitoring of the changes in the impedance response of the AZ31 and WE43 alloys in

Hank's solution under continuous injection of the molybdate inhibitor. Below, we discuss in detail the DEIS data analysis obtained during inhibitor injection (1 h, coupled with the DRT analysis) followed up by the prolonged corrosion resistance analysis (12 h). Due to the lower dynamics of the prolonged experiment, it was analyzed only by fitting with an electric equivalent circuit.

3.1. Corrosion inhibition by aqueous molybdate as a function of inhibitor concentration

To quantitively describe the inhibition efficiency of a corrosion inhibitor, direct comparison of the results of measurements performed in the solutions without and with the inhibitor are required. For this reason, corrosion monitoring was also performed in Hank's solution without the molybdate inhibitor. The detailed description of multisine DEIS impedance spectra in the reference Hank's solution without the inhibitor, their DRT analysis, and discussion of the corrosion mechanism are reported in our previous open access publication [28]. Therefore, in the present study we focus only on the solutions containing the molybdate inhibitor. The reference multisine DEIS impedance spectra of the AZ31 and WE43 Mg alloys obtained during 1 and 12 h of the exposure to Hanks's solution without the inhibitor are presented in Fig. S2 in the Supplementary information. Nyquist plots of the obtained DEIS spectra reveal net-like semicircle with the quality comparable to the traditional methods of impedance measurement.

The results of the DEIS measurements for1 h of the AZ31 and WE43 alloys in Hank's solution containing different amounts of sodium molybdate are shown in Fig. 1 (a, b). At each point of the measurement, the Nyquist spectra display the characteristic, dispersed capacitive loops. It can be seen that the chemistry of the examined Mg alloys to some extent affects the corrosion kinetics, represented by the shape of the impedance spectra, and have a crucial impact on the radii

of the Nyquist loops and their evolution in time, especially when the molybdate inhibitor is gradually added to the solution.

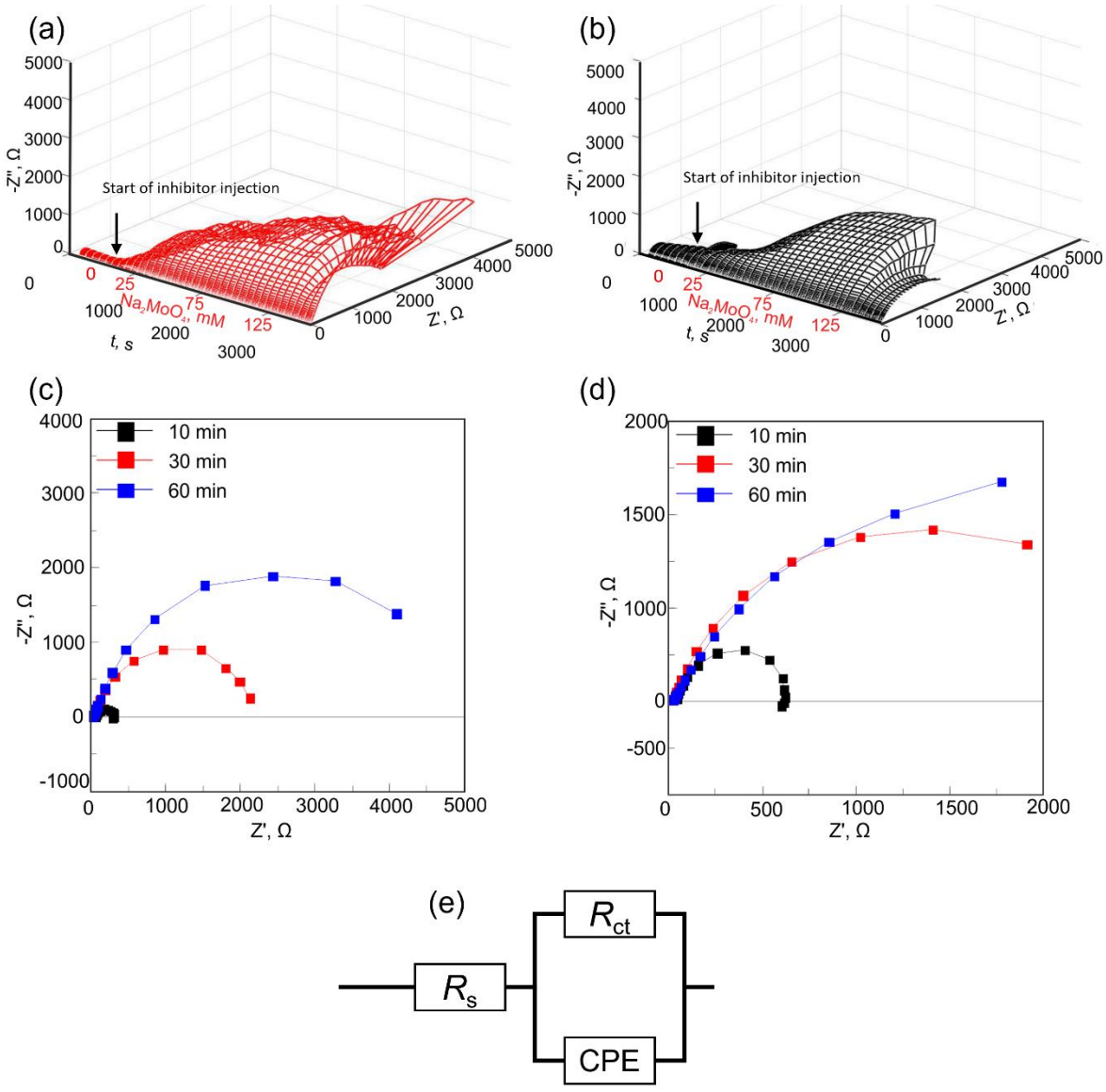

Fig. 1. Evolution of multisine DEIS spectra of (a, c) AZ31 and (b, d) WE43 Mg alloys as a function of the concentration of molybdate inhibitor in Hank's solution during 1 h-experiment. Panels (a, b) represent 3d Nyquist multisine DEIS plots as a function of time and panels (c, d) are selected 2d Nyquist multisine DEIS plots. (d) Equivalent circuit used for spectra fitting

The radii of impedance spectra in Nyquist representation of both examined Mg alloys were observed to increase as the injection of the molybdate inhibitor into Hank's solution began, when compared to the same time intervals in Hank's solution without the inhibitor (Fig. S2 in the Supplementary Information), with the maximum spectra radii upon reaching the concentration of 150 mM in the electrochemical cell. This behavior is explained by the blocking effect of the molybdate inhibitor. The obtained results indicate the high effectiveness of the molybdate inhibitor, and that the inhibition mechanism is concentration dependent. At the same time, relatively large concentrations of the inhibitor in the solution are required. This coincides well with our previous data on the corrosion inhibition of the AZ31 and WE43 Mg alloys by aqueous molybdate in 0.05 M NaCl solutions [21,22].

The obtained multisine impedance data were analyzed by fitting to an equivalent circuit (EEC) shown in Fig. 1e. In the case of Mg alloys, rather complex EECs are usually used for an accurate description of the occurring process [47]. In particular, low-frequency inductive loops should be considered in EECs to minimize the overestimation of the corrosion resistance of the Mg alloys [47]. Furthermore, the value of polarization resistance, R_p, is generally preferable to be analyzed. This approach was utilized in our previous studies of the AZ31 and WE43 alloys [21–23,48]. However, in the case of the DEIS measurements discussed in the present contribution, several limitations should be considered during the data analysis. originating from limiting the perturbation signal in the low-frequency range down to 0.7 Hz. Following these limitations and the shape of the multisine DEIS impedance spectra, a simple modification of the Randles circuit was used. In this circuit, R_s represents the solution resistance, R_{ct} represents the charge transfer resistance, and constant phase element (CPE) represents a capacitive response of the electrical double layer and an absorbed layer to properly introduce the electric heterogeneity of the partially protected electrode surface. The impedance of the CPE can be expressed as:

$$Z_{\mathrm{CPE}} = 1/(Q[j\omega]^n), \quad (1)$$

where Q is the CPE constant, j is the imaginary unit, ω is the angular frequency, and n is the CPE exponent. The exponent n usually describes the degree of the surface heterogeneity.

The parameters of the used EEC extracted from the multisine DEIS spectra measured in the first hour of the experiment are shown in Fig. 2. In this case, each spectrum was obtained at a different concentration of Na_2MoO_4 in the solution. Since the rate of the inhibitor injection was kept constant (Fig. S1 in the Supplementary Information) and the time required to obtain each spectrum depends on the lowest frequency applied (0.7 Hz), it is possible to assign each registered spectrum to the concentration of the molybdate inhibitor in Hank's solution. Therefore, the fitting data in Fig. 2 was recalculated to show the parameters of the used EEC as a function of the molybdate concentration in the solution.

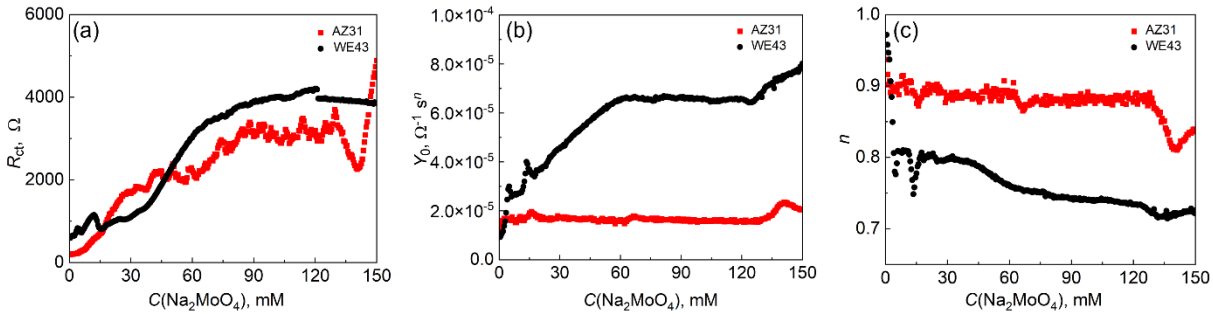

Fig. 2. Evolution of parameters of the used EEC (Fig. 1e) during 1 h immersion of AZ31 and WE43 Mg alloys in Hank's solution as a function of inhibitor concentration

The addition of the molybdate inhibitor into Hank's solution resulted in an increase in the values of the charge transfer resistance R_{ct}, comparing to the results obtained in the same time frames without the inhibitor (Fig. S3 in the Supplementary Information), proving the formation of a surface protective layer (Fig. 2a). The highest value of R_{ct} corresponds to the WE43 alloy in Hank's solution additionally containing ca. 120 mM of the molybdate inhibitor. At relatively high

concentrations of the inhibitor (ca. 120–130 mM), a drop in the values of R_{ct} was noted for both AZ31 and WE43 Mg alloys. It is in good accordance with the results of the classical EIS and polarization measurements described in our previous publications [21,22]. This decrease in the surface resistance can be explained by the excessive thickness of the formed molybdate-rich layer on the surface of Mg alloys. This may cause the occurrence of microcracks in the microstructure of the protective layer and its partial delamination from the surface. The change in the parameter *Q* of the CPE element showed that the CPE constant increased in the case of the WE43 alloy but remained almost constant for the AZ31 alloy (Fig. 2b). The *n* parameter of the CPE decreased for both alloys (Fig. 2c) as the concentration of the inhibitor in Hank's solution increased.

Knowledge about the instantaneous concentration of the molybdate inhibitor in the examined solutions at a given time point and corresponding impedance parameters in the solutions with and without the inhibitor can be used for calculation of the inhibition efficiency, *IE*, according to the following equation:

$$IE = (1 - R_{ct}^{0} / R_{ct}) \times 100\% \quad (2)$$

where R_{ct}^{0} is the charge transfer resistance measured in the solution without an inhibitor. The values of R_{ct}^{0} for corrosion of the AZ31 and WE43 Mg alloys in Hank's solution without the inhibitor were taken from our previous study [28] and are shown as Fig. S2 in the Supplementary Information. The calculated values of *IE* are shown in Fig. 3. It can be seen that *IE* gradually increases with an increase in the concentration of the inhibitor in Hank's solution. Fluctuations in *IE* at low inhibitor concentrations are connected with only partial coverage of the surface with the inhibitor and high dynamics of the system. The highest inhibition efficiency varied in the range of 80–90% and was higher for the WE43 alloy at concentrations of the molybdate inhibitor above 45 mM. Interestingly, the *IE* of molybdate dropped, especially for the AZ31 alloy, when approaching

the highest examined concentration of 150 mM, which is in line with the results obtained for R_{ct} (Fig. 2a). This behavior probably originates from the excessive thickness of the formed inhibitor layer, which may cause microcracks (later observed in SEM images) and delamination of the protective layer [21,49].

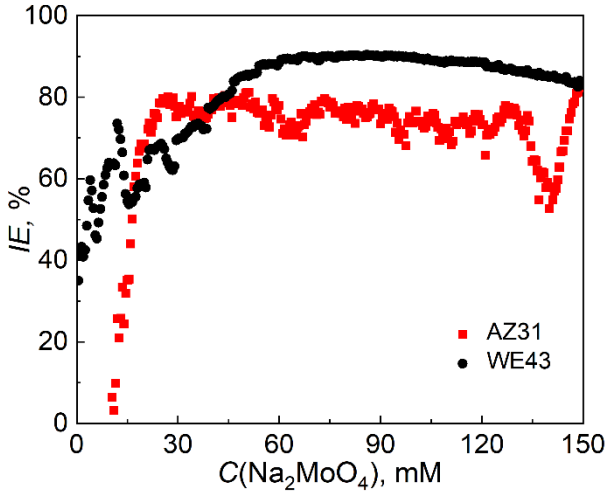

Fig. 3. Inhibition effectiveness of aqueous molybdate towards AZ31 and WE43 Mg alloys as a function of molybdate concentration recorded during 1 h immersion in Hank's solution

To get further inside into the kinetics of the electrochemical processes occurring during corrosion of magnesium alloys in Hank's solution in the presence of the molybdate inhibitor, the distribution of relaxation times (DRT) method was used to analyze the DEIS data. For the first 10 min of electrode conditioning, before the corrosion inhibitor injection, the corrosion process of both alloys is represented by a single process, τ_1, as illustrated in Fig. 4(a, b), in agreement with previous studies [28]. In the initial stage, corrosion proceeds by the dissolution of the Mg matrix. The mechanism of the process can be generally expressed by reactions (3, 4). Fast kinetics of this process consequence in the absence of secondary time constants in the analyzed spectra.

$$Mg \rightarrow Mg^{2+} + 2e \quad (3)$$

$$2H_2O + 2e \rightarrow H_2 + 2OH^- \quad (4)$$

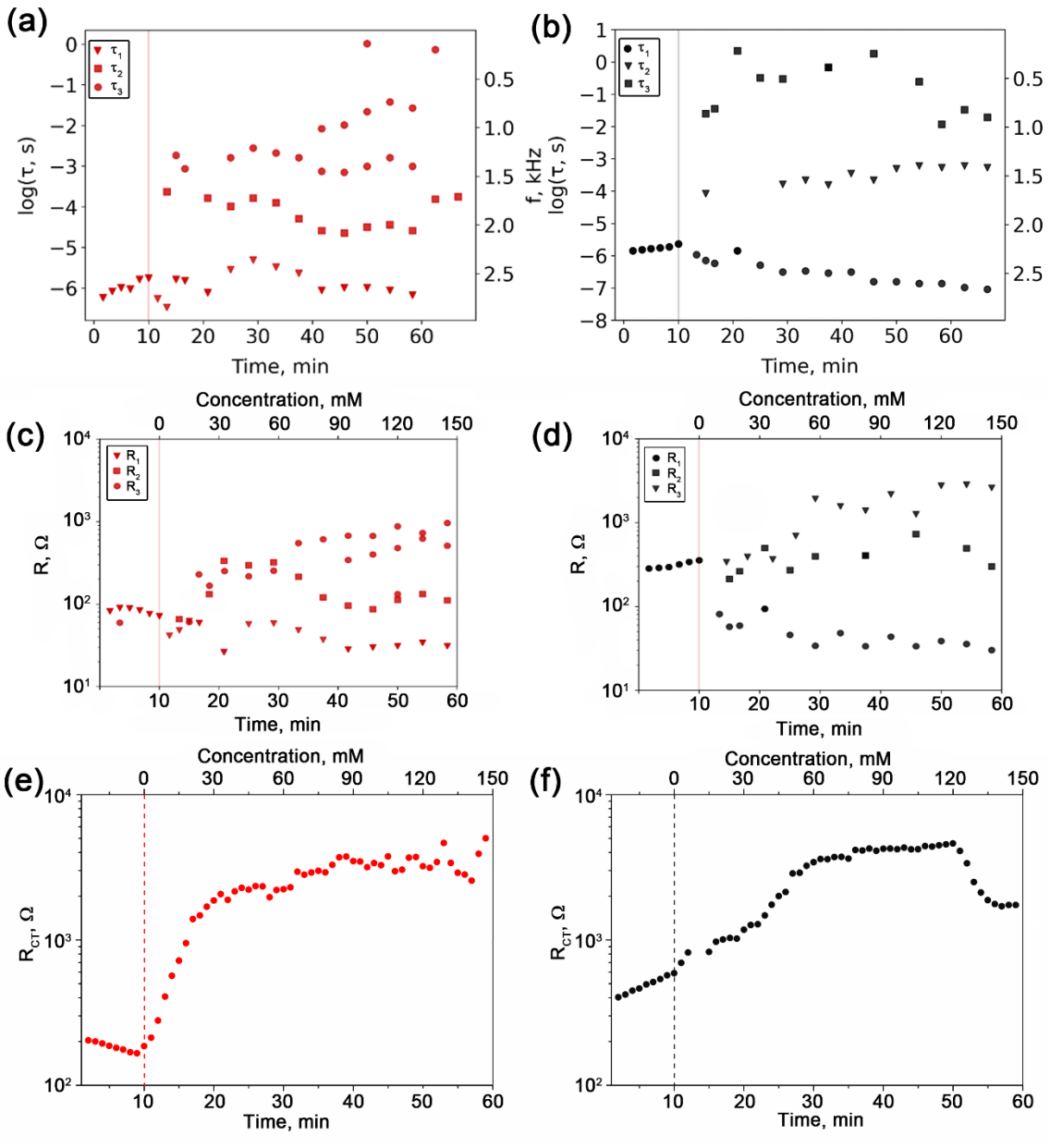

Fig. 4. Evolution of (a, b) DRT time constants, (c, d) distribution of resistances, and (e, f) calculated R_{ct} values for AZ31 (a, c, e) and WE43 (b, d, f) alloys. Vertical dashed line indicates moment of the beginning of the inhibitor injection

The injection of the corrosion inhibitor significantly complicates the charge transfer at the electrode/electrolyte interface as it is represented by the appearance of at least two additional time constants. This effect is visible from the very first moments, testifying high energy of molybdate ions adsorption toward the Mg alloys surface. These time constants, τ_2 and τ_3, are several orders of magnitude (approx. 2 and 4, respectively) compared to the initial process τ_1. Higher times needed to respond to impedimetric perturbation allow concluding the decrease of Mg oxidation kinetics even at low inhibitor concentrations. The appearance of these processes should be interpreted as the growth of the molybdate adsorption layer at the metal surface. Interestingly, the τ_3 process shows high levels of fluctuations, in particular referring to the WE43 alloy. Its origin is speculative, and its appearance might be connected to the secondary processes occurring with the intermetallic particles or the appearance and repassivation of the active-passive cells. Nonetheless, its presence constitutes evidence of system non-stationarity, where proper EEC utilization might be ambiguous.

One should also consider that the low-frequency limit utilized in multisine DEIS measurements (0.7 Hz) neglects the direct observation of the diffusion processes or adsorption of corrosion intermediates [21,47] typically seen in low-frequency regimes [27]. At the same time, it allows performing the measurement instantaneously, excluding ambiguities and artifacts and minimizing the error caused by system non-stationarity or the necessity of fitting with EECs. Furthermore, as described by Wysocka et al. [30], dynamic change of the surface coverage, θ, of the Mg alloys by the layer of the inhibitor during the DEIS measurements results in the overlapping of time-constants in the frequency domain and an increase in capacitance dispersion.

Resistance of the process can be calculated by integration of a field under a DRT peak. Correspondingly, capacitance can be calculated by dividing resistance value by a corresponding time constant. The resistances (R) of each time-constant are shown in Fig. 4(c, d). The addition of

361 the molybdate inhibitor into Hank's solution resulted in an overall increase in the resistance values.
362 The appearance of two additional time constants, τ_2 and τ_3, whose resistances surpass this of the
363 process P1 is proof of the formation of a surface protective layer (Fig. 4a). In turn, processes P2
364 and P3 were provisionally assigned to the adsorption of the molybdate ions on the surface and
365 formation of a protective layer of the inhibitor. The charge transfer resistance R_{ct} through the
366 electrode/electrolyte interphase calculated based on the DRT analysis can be evaluated as a sum of
367 the resistances of all three processes P1, P2, and P3 (see Fig. 4e, f).
368
369 **3.2. Corrosion inhibition by aqueous molybdate as a function of exposure time**
370 Further analysis was focused on the long-term (12 h) multisine DEIS measurements, which
371 were performed in Hank's solution on the same samples after the final concentration of the
372 molybdate inhibitor reached 150 mM. The obtained DEIS spectra are shown in Fig. 5. A significant
373 drop in the spectra radii was observed for the AZ31 alloy after ca. 3 h of exposure, while for the
374 WE43 alloy only a small drop was noted after 10 h of the experiment. Fitting of the obtained data
375 was performed using the same equivalent circuit shown in Fig. 1e.
376 The evolution of the circuit parameters in time is presented in Fig. 6. The R_{ct} followed the trend of
377 the spectra radii and was decreasing for the AZ31 alloy for the first 3 h of the experiment and then
378 was gradually increasing. In the case of the WE43 alloy, this parameter was increasing up to 10 h
379 of the experiment, and then started to decrease. The fluctuations of the capacitive parameter Y (Fig.
380 6b), especially for the WE43 alloy indicate instability of the surface passive film, which might be
381 associated with the occurrence of microcracks [21], which results in the initiation of local corrosion
382 attack and the formation of micropits on the surface. The parameter n gradually decreased for both
383 samples (Fig. 6c), yet its values are generally lower in case of the WE43 alloy, which might testify

for larger heterogeneities appearing at the surface or layer morphology or the discontinuity of the adsorbed layer. The latter case is less likely due to high charge transfer resistance offered by this alloy throughout all the exposure duration. Typically, when *n* is close to 0.5, the CPE corresponds to the diffusion process, which might suggest effective surface passivation.

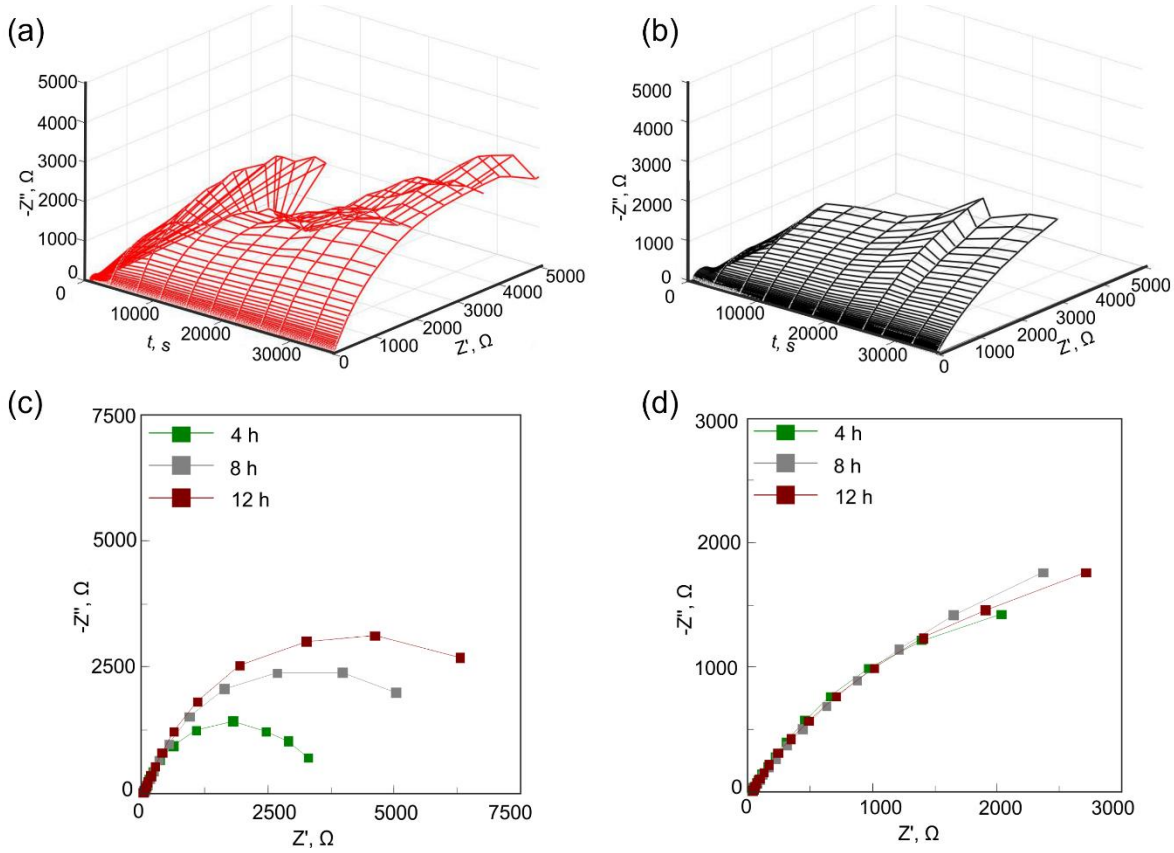

Fig. 5. Evolution of multisine DEIS spectra of (a, c) AZ31 and (b, d) WE43 Mg alloys as a function of the exposure time in Hank's solution containing 150 mM of molybdate inhibitor. Panels (a, b) represent 3d Nyquist multisine DEIS plots as a function of time and panels (c, d) are selected 2d Nyquist multisine DEIS plots

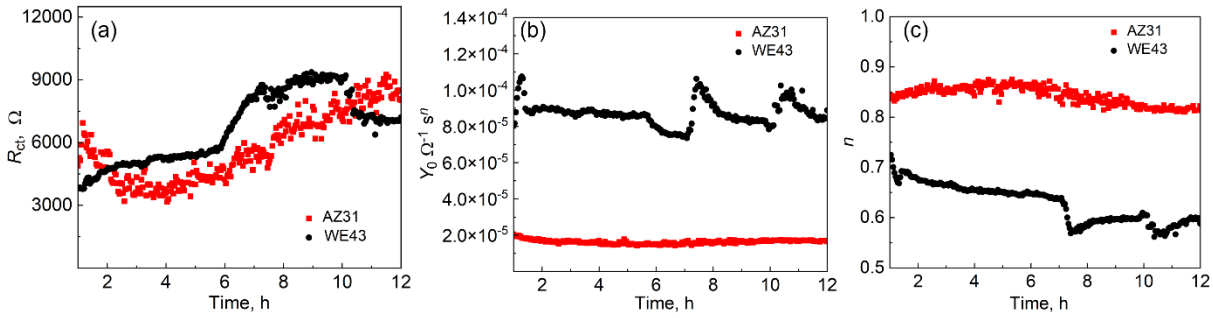

Fig. 6. Evolution of parameters of the used EEC (Fig. 1e) during 12 h immersion of AZ31 and WE43 Mg alloys in Hank's solution containing 150 mM of molybdate inhibitor

Comparison of the obtained data with the results of the experiments in Hank's solution without the inhibitor (Fig. S2 in the Supplementary Information) allowed to calculate the values of *IE*, shown in Fig. 7. The *IE* of aqueous molybdate towards the AZ31 alloy decreased with time and was fluctuating around the values of 40–60%, while for the WE43 alloy inhibition effectiveness was much more stable and kept around 80% for ca. 7 h, with further decrease to ca. 60%.

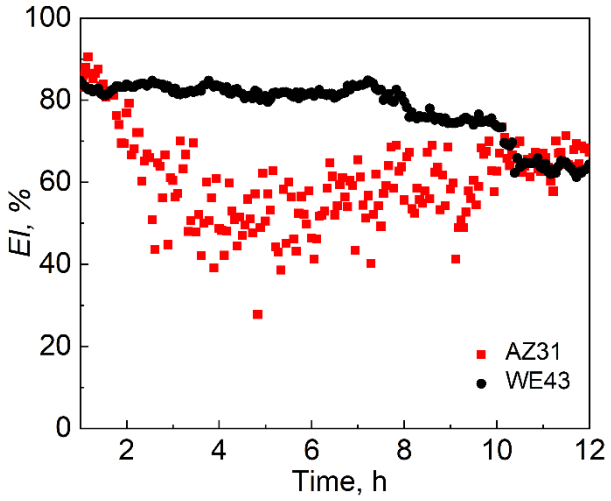

Fig. 7. Inhibition effectiveness of aqueous molybdate towards AZ31 and WE43 Mg alloys as a function of time recorded during 12 h immersion in Hank's solution containing 150 mM of Na_2MoO_4

Analyzing the impedance data and *IE* values with prolonged exposure leads to the conclusion that the inhibition efficiency offered by the molybdates remains high and offers a very competitive corrosion protection mechanism. In conclusion, multisine DEIS experiments demonstrate good inhibition efficiency of molybdate toward suppression of corrosion of both the AZ31 and WE43 alloys in Hank's solution.

3.3. Post corrosion surface examination

To further examine the mechanism of the corrosion protection of the AZ31 and WE43 alloys by aqueous molybdate in Hank's solution, *ex situ* SEM, EDX, and XPS measurements were performed. In this case, additional samples were prepared. To examine the difference in the composition of the surface layers, analyses were performed after 1 and 24 h of exposure to the examined solutions. The 24 h interval was selected to examine prolonged corrosion attack.

The surface morphologies of the AZ31 and WE43 alloys after exposure to the examined solutions are shown in Fig. 8. In the case of the AZ31 alloy, a thin passive layer of the inhibitor without visible microcracks was formed on the surface. Line defects seen in the images originate from the grinding procedure. However, no clear sign of corrosion areas was seen in the SEM images after 1 or 24 h of corrosion exposure. The surface morphology was clearly different in the case of the WE43 alloy. Almost the whole surface was covered by a passivating Mo-containing layer already after 1 h of exposure. The surface coverage of the Mo-based layer remained constant after 24 h of exposure. Some spots with larger microcracks in the passivating layer were observed. Such cracks in the passive layer are most probably caused by the internal stress of the layer due to its excessive thickness and evaporation of water from the surface. This feature is well-known for thick surface layers [23,50,51], and was also observed in the case of the AZ31 and WE43 alloys exposed to molybdate-cotaining NaCl solutions [21,22]. Nevertheless, these microcracks will not

result in permanent loss of corrosion protection as inhibitor ions in the solution can form a new protective layer in the areas of the surface defects, as can be seen from the results of the multisine impedance measurements (Fig. 5). Optical images of the surface (Fig. 8) also suggested smaller corrosion attack in the case of the inhibited solution compared to the uninhibited solution (Fig. S4 in the Supplementary information).

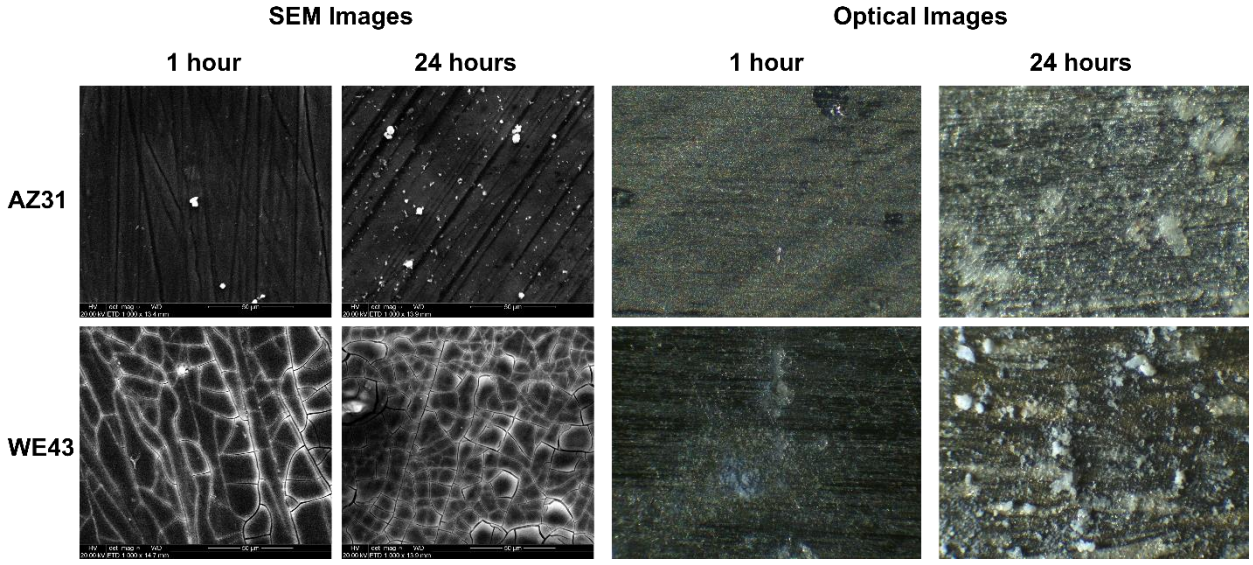

Fig. 8. Surface morphology of the AZ31 and WE43 alloys after 1 and 24 h exposure to Hank's solution with 150 mM of Na_2MoO_4 inhibitor.

The point EDX analysis of the surface of both alloys showed that the surface layer is primarily composed of Mg, O, and Mo. The content of Mo after 1 h of exposure was 0.9–1.2 and 1.4–4.3 wt.% for the AZ31 and WE43 alloys, respectively. After 24 h of corrosion testing in Hank's solution containing 150 mM of the molybdate inhibitor, the content of Mo varied in the range of 1.3–3.3 and 1.6–7.4 wt.% for the AZ31 and WE43 alloys, respectively. The relative Mo/O ratio cannot be estimated reliably from the EDX data since the surface layer also contains hydrated Mg compounds with varying stoichiometry [21]. However, EDX data clearly supports the multisine

impedance measurements data and confirms that molybdate is able to form a surface layer on the surface of the AZ31 and WE43 alloys.

To analyze the chemical state of the surface of the AZ31 and WE43 alloys after short and long-term corrosion experiments, XPS spectra were obtained. The survey XPS spectra of all samples are shown in Fig. S5 in the Supplementary Information. The signals from Mg, O, C, P, Al, Ca, Mo, Cl, and Na were observed in the Al survey spectra. High-resolution XPS spectra of the selected elements are presented in Fig. 9. After 1 h of corrosion, the high-resolution XPS spectra in the energy range corresponding to Mg 1s contained three components (Fig. 9a), which were assigned to the $MgO/Mg(OH)_2$ surface film (components $Mg_{(1)}$ at ca. 1304.5 eV (MgO) and $Mg_{(2)}$ at ca. 1301.8 eV ($Mg(OH)_2$)) and $MgCO_3$ (component $Mg_{(3)}$ at ca. 1306.2 eV). After 24 h of corrosion experiments, the component $Mg_{(1)}$ assigned to the MgO surface film dominated in the Mg 1s spectra.

The high-resolution XPS spectra in the energy range corresponding to Mo 3d were deconvoluted into two doublets with the spectrum of the AZ31 alloy after 24 h of corrosion experiments additionally showing the third doublet (Fig. 9b). However, precise peak identification for molybdenum compounds is not so straightforward. In aqueous solutions, molybdenum can form numerous compounds [51,52], with many of them showing the same or very close binding energies. Generally, larger binding energy in XPS measurements corresponds to an increase in the oxidation state of Mo in its compounds. In the case of Mg alloys, it is expected that more than one molybdenum compound is present in the surface layer. Based on this, XPS spectra were employed to assign oxidation states of Mo compounds in the surface passive film. The component $Mo_{(1)}$ with the $3d_{5/2}$ peak at 230.7 eV was assigned to Mo(V) compounds, usually observed in the composition of Mo-rich protective surface layers [21,22,33,53]. The $Mo_{(2)}$ component with the $3d_{5/2}$ peak at 232.6 eV corresponds to the electronic states of Mo(VI) compounds [51,54,55]. In the case of the

AZ31 alloy after 24 of corrosion in Hank's solution, the $Mo_{(3)}$ component with the $3d_{5/2}$ peak at 232.0 eV was observed, which was also assigned to the electronic states of Mo(VI). The lower binding energy of the main Mo component after 24 h of corrosion of the AZ31 alloy compared to the WE43 alloy may suggest that a mixed Mo(V)-Mo(VI) layer, which was formed on the surface of the AZ31 alloy has a larger fraction of Mo(V) species.

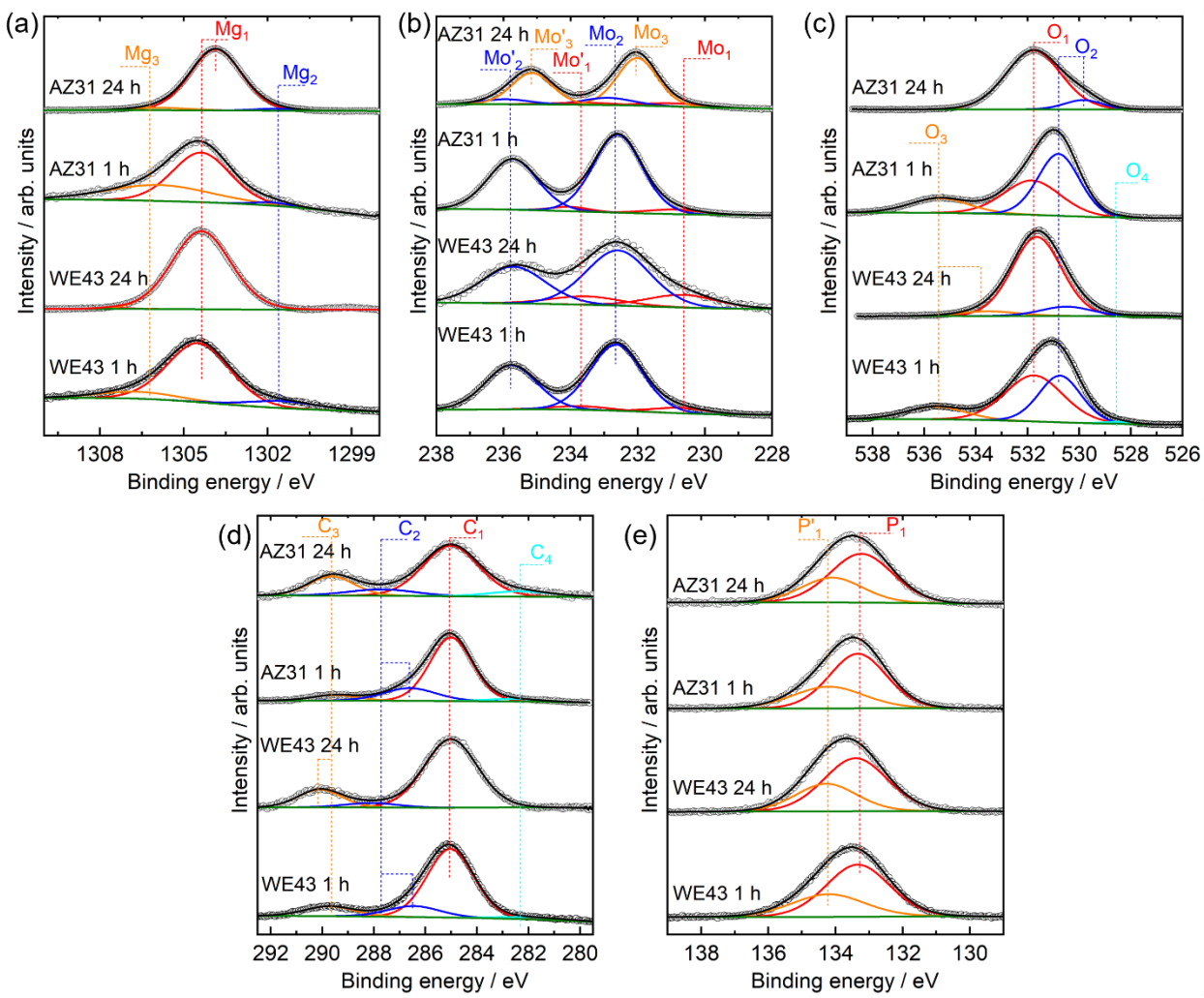

Fig. 9. High-resolution XPS spectra in the binding energy range of (a) Mg 1s, (b) Mo 3d, (c) O 1s, (d) C 1s, and (e) P 2p of AZ31 and WE43 Mg alloys after 1 and 24 h of corrosion in Hank's solution containing 150 mM of Na_2MoO_4

The high-resolution XPS spectra in the energy range corresponding to O 1s are of a complex nature but several distinct features can be observed (Fig. 9c). The component $O_{(1)}$ located at 531.8

eV was assigned to $MgO/Mg(OH)_2$ and/or CaO [22]. In turn, the component $O_{(2)}$ was assigned to Mo–O species, MgO, and possibly phosphates [56–58]. Interestingly, the position of this peak was constant (530.8 eV) for all measured samples except of the AZ31 alloy after 24 h of corrosion monitoring (529.8 eV). It indicates the change in the composition of the surface protective film, which is also supported by the XPS data of Mo species, discussed below. The origin of the $O_{(3)}$ and $O_{(4)}$ components is not so straightforward. The component $O_{(3)}$ was assigned to surface carbonates or other components of the Hank's solution, while the component $O_{(4)}$ was identified as surface oxides originating from IMPs elements.

The high-resolution spectra obtained in the C 1s region (Fig. 9d) were deconvoluted into four components with their assignment strongly depending on the exposure time. The first component $C_{(1)}$ located at 285.0 eV, assigned to C–C/C–H bonds in organic compounds and contaminations [59], was found in all samples. The second component, $C_{(2)}$, was assigned to single C–O (after 1 h of exposure) and double C=O (after 24 h of exposure) bonding, respectively. The next component, marked as $C_{(3)}$ located at 289.5 was assigned to carbonates. The last component, $C_{(4)}$, located at 282.3 eV, originated from the carbides, which might be a surface contamination due to polishing. The components $C_{(1)}$, $C_{(2)}$, and $C_{(4)}$ are mainly associated with surface contamination [60], while carbonates are a part of the surface film of corrosion products [21,22,61].

The P 2p spectrum for all samples was deconvoluted into one doublet with P $2p_{3/2}$ and P $2p_{1/2}$ binding energies of 133.3 and 134.1 eV (marked as P and P', respectively), assigned to phosphates (Fig. 9e) [62].

3.4. Mechanism of inhibition

In this section, we summarize the results obtained by multisine impedance, SEM, and XPS analyses and discuss the mechanism of the corrosion inhibition of the AZ31 and WE43 Mg alloys

by aqueous molybdate in Hank's solution. First, a brief description of the corrosion mechanisms of the AZ31 and WE43 alloys in Hank's solution without the molybdate inhibitor is required. These mechanisms are in detail discussed in our previous contribution [28] and here we briefly state their main steps. Corrosion of Mg alloys in Hank's solution proceeds rapidly and results in the formation of magnesium hydroxide and hydrogen gas according to Eqs. (3, 4).

In the case of Hank's solution, magnesium phosphates and carbonates can also precipitate on the surface of Mg alloys due to the interaction of released Mg^{2+} ions with the components of the corrosion medium. Nevertheless, the initially formed layer of corrosion products is porous and does not provide sufficient corrosion protection of the substrate. The cathodic activity of IMPs in the microstructure of the AZ31 and WE43 alloys [28,63] and the presence of Cl^- ions in Hank's solution result in the occurrence of pitting corrosion [22,28,63]. In the case of the WE43 alloy, the corrosion process has an additional step in the form of filiform corrosion, which initiates on the surface regions of cathodic IMPs [28,64,65].

Our results demonstrated that the introduction of Na_2MoO_4 into Hank's solution dramatically changes the corrosion behavior of the AZ31 and WE43 Mg alloys. No pitting or filiform corrosion was observed on the surface based on SEM images. Dissolved molybdate readily retards corrosion attack by forming a protective insoluble film on the metal surface. Importantly, in previous studies in 0.05 M NaCl solutions [21,22], low molybdate concentrations (up to 10 mM) resulted in an increase in the corrosion rate of the AZ31 and WE43 alloys after 30 min of exposure to a corrosive medium due to only partial coverage of the active surface areas. This phenomenon was not observed in the present study for the WE43 alloy, since R_{ct} and *IE* were gradually increasing with the addition of the inhibitor in Hank's solution (Figs. 2, 3). However, it was confirmed in the case of the AZ31 inhibitor, for which the protection level was generally lower and negative values of *IE* were observed for concentrations below ca. 15 mM. Therefore, in the

discussion below we assume a concentration of the molybdate inhibitor in the system high enough to provide reliable corrosion inhibition.

Generally, several types of poly- and monomolybdates can be found in an aqueous solution depending on its pH [33,52]. The change in the pH and the OCP of the studied Mg alloys as a function of time is shown in Fig. S6 in the supplementary information. The initial pH of Hank's solution was in the range of 7.3–7.5 with a maximum bulk pH of ca. 7.9 after 12 h of corrosion monitoring. In these conditions, only monomolybdates MoO_4^{2-} are presented in aqueous solutions. Our multisine DEIS data confirmed that the first stage in the mechanism of the corrosion inhibition is the rapid adsorption of molybdate anions on the surface of the AZ31 and WE43 alloys, resulting in a rapid increase in the charge transfer resistance due to the formation of the surface film. At first, isolated molybdate monomers are adsorbed on the surface. As the bulk concentration of molybdate ions increases, adsorption of excess molybdate would result in the formation of hydrated polymolybdates through condensation reactions of monomers [21].

Molybdates have a rather low oxidizing capacity and their aqueous solutions are stable [66]. Nevertheless, our XPS data (Fig. 9) confirmed the presence of mixed valence Mo(VI) and Mo(V) species on the top surface layer. Previous studies [21,22,51,66] have shown that this mixed-valence layer is formed in the second stage of inhibition through the reduction of polymerized monomolybdate ions. However, our observations suggest that this stage is greatly affected by the microstructure of the Mg alloys. A thick molybdate-containing passive layer was formed on the surface of the WE43 alloy, while that on the surface of the AZ31 layer was not so thick and did not contain visible defects. It is also confirmed by the difference in the inhibition efficiency, which was lower for the AZ31 alloy. This phenomenon can be explained by the presence of Al in the composition of the AZ31 alloy and its low catalytic activity towards the reduction of molybdenum

557 species. Molybdates could be adsorbed on the surface of Al-rich IMPs. However, the low cathodic
558 activity of Al_2O_3 does not promote the initial reduction of the adsorbed Mo(VI) species, thus the
559 presence of only a thin layer of polymerized Mo(VI) is favorable. These assumptions are also
560 supported by the XPS data after 24 h of corrosion in Hank's solution containing 150 mM of
561 molybdate (Fig. 9), with the relative ratio of Mo(VI)/Mo(V) species on the surface being ca. 11.5/1
562 and 4/1 for the AZ31 and WE43 alloys, respectively. The same behavior was observed in the case
563 of the corrosion inhibition of pure Al and the AA6063 Al alloy by aqueous molybdate [33,67]. This
564 feature is even more prominent in the case of the AZ91 Mg alloy, which contains a larger fraction
565 of Al compared to the AZ31 alloy (not shown in the present contribution).

566 The occurrence of a large number of microcracks in the surface film over the WE43 alloy
567 suggests that the reduction of the inhibitor is not self-limiting. However, active surface sites of this
568 alloy were blocked during the first injection of inhibitor and initial adsorption of monomolybdates.
569 Therefore, no significant effects would be expected due to the further reduction of the surface layer
570 suggesting that initial absorption of monomolybdates and their high concentration in the corrosive
571 medium impart corrosion protection of the WE43 alloy in Hank's solution, providing long-time
572 high inhibition efficiency.

573

574 **4. Conclusions**

575 In this work, the effect of molybdate on the corrosion processes of the AZ31 and WE43
576 magnesium alloys in Hank's solution was examined. The use of the multisine dynamic
577 electrochemical impedance spectroscopy and distribution of relaxation times (DRT) analysis
578 allowed for instantaneous monitoring of the inhibition efficiency in time. The DRT analysis
579 confirmed that the addition of the molybdate inhibitor into Hank's solution resulted in the
580 resistance values and the appearance of two additional processes, assigned to the adsorption of the

molybdate ions on the surface and formation of a protective layer of the inhibitor. Electrochemical data revealed that aqueous molybdate leads to a significant decrease in the corrosion rate of the Mg alloys in Hank's solution. High corrosion protection effectiveness of molybdate was correlated with the surface film composition, examined by EDX and XPS. The formed surface film consists of mix-valence Mo(VI)–Mo(V) species. A combination of electrochemical and spectroscopic data allowed to propose the mechanism of the corrosion inhibition by aqueous molybdate based on the adsorption of molybdate anions on the surface of Mg alloys with formation of a Mo(VI)-Mo(V) protective layer, which suppresses further corrosion attack.

Declarations of interest

The authors declare that they have no known competing financial interests or personal relationships that could have appeared to influence the work reported in this paper.

Data availability

The raw/processed data required to reproduce the findings of this study are available from the corresponding authors upon reasonable request.

Acknowledgments

Dzmitry S. Kharytonau gratefully acknowledges financial support from the National Science Centre (Poland) under research Grant Sonatina no. 2021/40/C/ST5/00266. This work was also supported by Gdańsk University of Technology under the Aurum Supporting International Research Team Building – 'Excellence Initiative – Research University' (2/2021/IDUB/II.1.3).

CRediT authorship contribution statement

Maria A. Osipenko: Data curation, Formal analysis, Investigation.

Jakub Karczewski: Formal analysis, Methodology, Supervision, Writing – original draft, Writing – review & editing.

Michał Dominów: Data curation, Formal analysis, Software, Validation, Visualization, Writing – original draft

Marta Prześniak-Welenc: Investigation.

Jacek Gurgul: Investigation.

Iryna I. Kurilo: Supervision, Writing – review & editing.

Jacek Ryl: Conceptualization, Formal analysis, Funding acquisition, Investigation, Methodology, Project administration, Resources, Supervision, Visualization, Writing – original draft, Writing – review & editing.

Dzmitry S. Kharytonau: Conceptualization, Formal analysis, Funding acquisition, Investigation, Methodology, Project administration, Resources, Supervision, Visualization, Writing – original draft, Writing – review & editing.

References

[1] M. Esmaily, J.E. Svensson, S. Fajardo, N. Birbilis, G.S. Frankel, S. Virtanen, R. Arrabal, S. Thomas, L.G. Johansson, Fundamentals and advances in magnesium alloy corrosion, Prog. Mater. Sci. 89 (2017) 92–193. https://doi.org/10.1016/j.pmatsci.2017.04.011.

[2] R. Miranda, Surface reinforcements of light alloys, in: Surf. Modif. by Solid State Process., Elsevier, 2014: pp. 113–152. https://doi.org/10.1533/9780857094698.113.

[3] R.B. Heimann, Magnesium alloys for biomedical application: Advanced corrosion control through surface coating, Surf. Coatings Technol. 405 (2021) 126521. https://doi.org/10.1016/j.surfcoat.2020.126521.

[4] P. Tong, Y. Sheng, R. Hou, M. Iqbal, L. Chen, J. Li, Recent progress on coatings of biomedical magnesium alloy, Smart Mater. Med. 3 (2022) 104–116. https://doi.org/10.1016/j.smaim.2021.12.007.

[5] M. Liu, J. Wang, S. Zhu, Y. Zhang, Y. Sun, L. Wang, S. Guan, Corrosion fatigue of the extruded Mg–Zn–Y–Nd alloy in simulated body fluid, J. Magnes. Alloy. 8 (2020) 231–240. https://doi.org/10.1016/j.jma.2019.09.009.

[6] E. Lukyanova, N. Anisimova, N. Martynenko, M. Kiselevsky, S. Dobatkin, Y. Estrin, Features of in vitro and in vivo behaviour of magnesium alloy WE43, Mater. Lett. 215 (2018) 308–311. https://doi.org/10.1016/j.matlet.2017.12.125.

[7] S. Prasadh, S. Raguraman, R. Wong, M. Gupta, Current Status and Outlook of Temporary Implants (Magnesium/Zinc) in Cardiovascular Applications, Metals (Basel). 12 (2022) 999. https://doi.org/10.3390/met12060999.

[8] M. He, L. Chen, M. Yin, S. Xu, Z. Liang, Review on magnesium and magnesium-based alloys as biomaterials for bone immobilization, J. Mater. Res. Technol. 23 (2023) 4396–4419. https://doi.org/10.1016/j.jmrt.2023.02.037.

[9] M. Ascencio, M. Pekguleryuz, S. Omanovic, An investigation of the corrosion mechanisms of WE43 Mg alloy in a modified simulated body fluid solution: The influence of immersion time, Corros. Sci. 87 (2014) 489–503. https://doi.org/10.1016/j.corsci.2014.07.015.

[10] M. Deng, L. Wang, D. Höche, S. V Lamaka, C. Wang, D. Snihirova, Y. Jin, Y. Zhang, M.L. Zheludkevich, Approaching "stainless magnesium" by Ca micro-alloying, Mater. Horizons. 8 (2021) 589–596. https://doi.org/10.1039/D0MH01380C.

[11] D. Bairagi, S. Mandal, A comprehensive review on biocompatible Mg-based alloys as temporary orthopaedic implants: Current status, challenges, and future prospects, J. Magnes. Alloy. 10 (2022) 627–669. https://doi.org/10.1016/j.jma.2021.09.005.

[12] Y.F. Zheng, X.N. Gu, F. Witte, Biodegradable metals, Mater. Sci. Eng. R Reports. 77 (2014) 1–34. https://doi.org/10.1016/j.mser.2014.01.001.

[13] W. Yuan, D. Xia, S. Wu, Y. Zheng, Z. Guan, J. V. Rau, A review on current research status of the surface modification of Zn-based biodegradable metals, Bioact. Mater. 7 (2022) 192–216. https://doi.org/10.1016/j.bioactmat.2021.05.018.

[14] H. Pan, K. Pang, F. Cui, F. Ge, C. Man, X. Wang, Z. Cui, Effect of alloyed Sr on the microstructure and corrosion behavior of biodegradable Mg-Zn-Mn alloy in Hanks' solution, Corros. Sci. 157 (2019) 420–437. https://doi.org/10.1016/j.corsci.2019.06.022.

[15] H. Kalb, A. Rzany, B. Hensel, Impact of microgalvanic corrosion on the degradation morphology of WE43 and pure magnesium under exposure to simulated body fluid, Corros. Sci. 57 (2012) 122–130. https://doi.org/10.1016/j.corsci.2011.12.026.

[16] N.I. Zainal Abidin, B. Rolfe, H. Owen, J. Malisano, D. Martin, J. Hofstetter, P.J. Uggowitzer, A. Atrens, The in vivo and in vitro corrosion of high-purity magnesium and magnesium alloys WZ21 and AZ91, Corros. Sci. 75 (2013) 354–366. https://doi.org/10.1016/j.corsci.2013.06.019.

671 [17] D. Mei, S. V. Lamaka, X. Lu, M.L. Zheludkevich, Selecting medium for corrosion testing
672 of bioabsorbable magnesium and other metals – A critical review, Corros. Sci. 171 (2020)
673 108722. https://doi.org/10.1016/j.corsci.2020.108722.
674 [18] S. V. Lamaka, B. Vaghefinazari, D. Mei, R.P. Petrauskas, D. Höche, M.L. Zheludkevich,
675 Comprehensive screening of Mg corrosion inhibitors, Corros. Sci. 128 (2017) 224–240.
676 https://doi.org/10.1016/j.corsci.2017.07.011.
677 [19] B. Vaghefinazari, E. Wierzbicka, P. Visser, R. Posner, R. Arrabal, E. Matykina, M.
678 Mohedano, C. Blawert, M.L. Zheludkevich, S. V Lamaka, Chromate-Free Corrosion
679 Protection Strategies for Magnesium Alloys—A Review: Part III—Corrosion Inhibitors and
680 Combining Them with Other Protection Strategies, Materials (Basel). 15 (2022) 8489.
681 https://doi.org/10.3390/ma15238489.
682 [20] E. Wierzbicka, B. Vaghefinazari, M. Mohedano, P. Visser, R. Posner, C. Blawert, M.
683 Zheludkevich, S. Lamaka, E. Matykina, R. Arrabal, Chromate-Free Corrosion Protection
684 Strategies for Magnesium Alloys—A Review: Part II—PEO and Anodizing, Materials
685 (Basel). 15 (2022) 8515. https://doi.org/10.3390/ma15238515.
686 [21] D.S. Kharitonov, M. Zimowska, J. Ryl, A. Zieliński, M.A. Osipenko, J. Adamiec, A.
687 Wrzesińska, P.M. Claesson, I.I. Kurilo, Aqueous molybdate provides effective corrosion
688 inhibition of WE43 magnesium alloy in sodium chloride solutions, Corros. Sci. 190 (2021)
689 109664. https://doi.org/10.1016/j.corsci.2021.109664.
690 [22] M.A. Osipenko, D.S. Kharytonau, A.A. Kasach, J. Ryl, J. Adamiec, I.I. Kurilo, Inhibitive
691 Effect of Sodium Molybdate on Corrosion of AZ31 Magnesium Alloy in Chloride Solutions,
692 Electrochim. Acta. 414 (2022) 140175. https://doi.org/10.1016/j.electacta.2022.140175.
693 [23] M.A. Osipenko, A.A. Kasach, J. Adamiec, M. Zimowska, I.I. Kurilo, D.S. Kharytonau,
694 Corrosion inhibition of magnesium alloy AZ31 in chloride-containing solutions by aqueous

permanganate, J. Solid State Electrochem. (2023). https://doi.org/10.1007/s10008-023-05472-3.

[24] Z. Feng, B. Hurley, M. Zhu, Z. Yang, J. Hwang, R. Buchheit, Corrosion Inhibition of AZ31 Mg Alloy by Aqueous Selenite (SeO 3 2−), J. Electrochem. Soc. 166 (2019) C520–C529. https://doi.org/10.1149/2.0911914jes.

[25] Z. Feng, B. Hurley, J. Li, R. Buchheit, Corrosion Inhibition Study of Aqueous Vanadate on Mg Alloy AZ31, J. Electrochem. Soc. 165 (2018) C94–C102. https://doi.org/10.1149/2.1171802jes.

[26] S.A. Umoren, M.T. Abdullahi, M.M. Solomon, An overview on the use of corrosion inhibitors for the corrosion control of Mg and its alloys in diverse media, J. Mater. Res. Technol. 20 (2022) 2060–2093. https://doi.org/10.1016/j.jmrt.2022.08.021.

[27] L. Wang, D. Snihirova, M.D. Havigh, M. Deng, S. V. Lamaka, H. Terryn, M.L. Zheludkevich, Non-stationarity in electrochemical impedance measurement of Mg-based materials in aqueous media, Electrochim. Acta. 468 (2023) 143140. https://doi.org/10.1016/j.electacta.2023.143140.

[28] M.A. Osipenko, J. Karczewski, M. Dominów, M. Prześniak-Welenc, I. V. Makarava, I. Kurilo, D.S. Kharytonau, J. Ryl, Multisine impedimetric monitoring with an in-depth distribution of relaxation times analysis of WE43 and AZ31 magnesium alloys corrosion, Measurement. 222 (2023) 113683. https://doi.org/10.1016/j.measurement.2023.113683.

[29] J. Orlikowski, J. Ryl, M. Jarzynka, S. Krakowiak, K. Darowicki, Instantaneous Impedance Monitoring of Aluminum Alloy 7075 Corrosion in Borate Buffer with Admixed Chloride Ions, CORROSION. 71 (2015) 828–838. https://doi.org/10.5006/1546.

[30] J. Wysocka, M. Cieslik, S. Krakowiak, J. Ryl, Carboxylic acids as efficient corrosion inhibitors of aluminium alloys in alkaline media, Electrochim. Acta. 289 (2018) 175–192.

https://doi.org/10.1016/j.electacta.2018.08.070.

[31] J. Wysocka, S. Krakowiak, J. Ryl, Evaluation of citric acid corrosion inhibition efficiency and passivation kinetics for aluminium alloys in alkaline media by means of dynamic impedance monitoring, Electrochim. Acta. 258 (2017) 1463–1475. https://doi.org/10.1016/j.electacta.2017.12.017.

[32] J. Ryl, J. Wysocka, M. Cieslik, H. Gerengi, T. Ossowski, S. Krakowiak, P. Niedzialkowski, Understanding the origin of high corrosion inhibition efficiency of bee products towards aluminium alloys in alkaline environments, Electrochim. Acta. 304 (2019) 263–274. https://doi.org/10.1016/j.electacta.2019.03.012.

[33] D.S. Kharitonov, I. Dobryden, B. Sefer, J. Ryl, A. Wrzesińska, I. V. Makarova, I. Bobowska, I.I. Kurilo, P.M. Claesson, Surface and corrosion properties of AA6063-T5 aluminum alloy in molybdate-containing sodium chloride solutions, Corros. Sci. 171 (2020) 108658. https://doi.org/10.1016/j.corsci.2020.108658.

[34] A. Toschka, H. Möllmann, D. Hoppe, G. Poehle, L. van Meenen, M. Seidl, N. Karnatz, M. Rana, How Does the Biocompatibility of Molybdenum Compare to the Gold Standard Titanium?—An In Vivo Rat Model, Appl. Sci. 13 (2023) 6312. https://doi.org/10.3390/app13106312.

[35] A.R. Khan, N.S. Grewal, C. Zhou, K. Yuan, H.-J. Zhang, Z. Jun, Recent advances in biodegradable metals for implant applications: Exploring in vivo and in vitro responses, Results Eng. 20 (2023) 101526. https://doi.org/10.1016/j.rineng.2023.101526.

[36] M. Petrova, M. Bojinov, S. Zanna, P. Marcus, Mechanism of anodic oxidation of molybdenum in nearly-neutral electrolytes studied by electrochemical impedance spectroscopy and X-ray photoelectron spectroscopy, Electrochim. Acta. 56 (2011) 7899–7906. https://doi.org/10.1016/j.electacta.2010.12.022.

743 [37] D.G. Heijerick, S. Carey, The toxicity of molybdate to freshwater and marine organisms.
744 III. Generating additional chronic toxicity data for the refinement of safe environmental
745 exposure concentrations in the US and Europe, Sci. Total Environ. 609 (2017) 420–428.
746 https://doi.org/10.1016/j.scitotenv.2017.07.070.
747 [38] Toxicological Profile for Molybdenum, Agency for Toxic Substances and Disease Registry,
748 2020. https://www.atsdr.cdc.gov/ToxProfiles/tp212.pdf.
749 [39] J. Turnlund, W. Keyes, G. Peiffer, G. Chiang, Molybdenum absorption, excretion, and
750 retention studied with stable isotopes in young men during depletion and repletion, Am. J.
751 Clin. Nutr. 61 (1995) 1102–1109. https://doi.org/10.1093/ajcn/61.5.1102.
752 [40] A. Schauer, C. Redlich, J. Scheibler, G. Poehle, P. Barthel, A. Maennel, V. Adams, T.
753 Weissgaerber, A. Linke, P. Quadbeck, Biocompatibility and Degradation Behavior of
754 Molybdenum in an In Vivo Rat Model, Materials (Basel). 14 (2021) 7776.
755 https://doi.org/10.3390/ma14247776.
756 [41] K. Darowicki, P. Ślepski, Dynamic electrochemical impedance spectroscopy of the first
757 order electrode reaction, J. Electroanal. Chem. 547 (2003) 1–8.
758 https://doi.org/10.1016/S0022-0728(03)00154-2.
759 [42] J. Ryl, K. Darowicki, Impedance Monitoring of Carbon Steel Cavitation Erosion under the
760 Influence of Corrosive Factors, J. Electrochem. Soc. 155 (2008) P44.
761 https://doi.org/10.1149/1.2840619.
762 [43] K. Darowicki, Theoretical description of the measuring method of instantaneous impedance
763 spectra, J. Electroanal. Chem. 486 (2000) 101–105. https://doi.org/10.1016/S0022-
764 0728(00)00110-8.
765 [44] F. Gao, L. Han, Implementing the Nelder-Mead simplex algorithm with adaptive
766 parameters, Comput. Optim. Appl. 51 (2012) 259–277. https://doi.org/10.1007/s10589-010-

9329-3.

[45] Ryl, Brodowski, Kowalski, Lipinska, Niedzialkowski, Wysocka, Corrosion Inhibition Mechanism and Efficiency Differentiation of Dihydroxybenzene Isomers Towards Aluminum Alloy 5754 in Alkaline Media, Materials (Basel). 12 (2019) 3067. https://doi.org/10.3390/ma12193067.

[46] T.H. Wan, M. Saccoccio, C. Chen, F. Ciucci, Influence of the Discretization Methods on the Distribution of Relaxation Times Deconvolution: Implementing Radial Basis Functions with DRTtools, Electrochim. Acta. 184 (2015) 483–499. https://doi.org/10.1016/j.electacta.2015.09.097.

[47] A.D. King, N. Birbilis, J.R. Scully, Accurate electrochemical measurement of magnesium corrosion rates; A combined impedance, mass-loss and hydrogen collection study, Electrochim. Acta. 121 (2014) 394–406. https://doi.org/10.1016/j.electacta.2013.12.124.

[48] P. Nowak, M. Mosiałek, D.S. Kharitonov, J. Adamiec, A. Turowska, Effect of TIG Welding and Rare Earth Elements Alloying on Corrosion Resistance of Magnesium Alloys, J. Electrochem. Soc. 167 (2020) 131504. https://doi.org/10.1149/1945-7111/abb97e.

[49] D.S. Kharitonov, J. Sommertune, C. Örnek, J. Ryl, I.I. Kurilo, P.M. Claesson, J. Pan, Corrosion inhibition of aluminium alloy AA6063-T5 by vanadates: Local surface chemical events elucidated by confocal Raman micro-spectroscopy, Corros. Sci. 148 (2019) 237–250. https://doi.org/10.1016/j.corsci.2018.12.011.

[50] Z. Yong, J. Zhu, C. Qiu, Y. Liu, Molybdate/phosphate composite conversion coating on magnesium alloy surface for corrosion protection, Appl. Surf. Sci. 255 (2008) 1672–1680. https://doi.org/10.1016/j.apsusc.2008.04.095.

[51] H. Verbruggen, K. Baert, H. Terryn, I. De Graeve, Molybdate-phosphate conversion coatings to protect steel in a simulated concrete pore solution, Surf. Coatings Technol. 361

(2019) 280–291. https://doi.org/10.1016/j.surfcoat.2018.09.056.

[52] E.A. Nagul, I.D. McKelvie, P. Worsfold, S.D. Kolev, The molybdenum blue reaction for the determination of orthophosphate revisited: Opening the black box, Anal. Chim. Acta. 890 (2015) 60–82. https://doi.org/10.1016/j.aca.2015.07.030.

[53] P. Kwolek, Corrosion behaviour of 7075 aluminium alloy in acidic solution, RSC Adv. 10 (2020) 26078–26089. https://doi.org/10.1039/D0RA04215C.

[54] P.A. Spevack, N.S. McIntyre, A Raman and XPS investigation of supported molybdenum oxide thin films. 1. Calcination and reduction studies, J. Phys. Chem. 97 (1993) 11020–11030. https://doi.org/10.1021/j100144a020.

[55] O. Marin-Flores, L. Scudiero, S. Ha, X-ray diffraction and photoelectron spectroscopy studies of MoO2 as catalyst for the partial oxidation of isooctane, Surf. Sci. 603 (2009) 2327–2332. https://doi.org/10.1016/j.susc.2009.05.010.

[56] C.C. Chusuei, D.W. Goodman, M.J. Van Stipdonk, D.R. Justes, E.A. Schweikert, Calcium Phosphate Phase Identification Using XPS and Time-of-Flight Cluster SIMS, Anal. Chem. 71 (1999) 149–153. https://doi.org/10.1021/ac9806963.

[57] A. Hiji, T. Hanawa, M. Shimabukuro, P. Chen, M. Ashida, K. Ishikawa, Initial formation kinetics of calcium phosphate on titanium in Hanks' solution characterized using XPS, Surf. Interface Anal. 53 (2021) 185–193. https://doi.org/10.1002/sia.6900.

[58] B.M. Reddy, B. Chowdhury, E.P. Reddy, A. Fernández, An XPS study of dispersion and chemical state of MoO3 on Al2O3-TiO2 binary oxide support, Appl. Catal. A Gen. 213 (2001) 279–288. https://doi.org/10.1016/S0926-860X(00)00906-6.

[59] X. Chen, X. Wang, D. Fang, A review on C1s XPS-spectra for some kinds of carbon materials, Fullerenes, Nanotub. Carbon Nanostructures. 28 (2020) 1048–1058. https://doi.org/10.1080/1536383X.2020.1794851.

[60] H. Fang, C. Wang, S. Zhou, G. Li, Y. Tian, T. Suga, Exploration of the enhanced performances for silk fibroin/sodium alginate composite coatings on biodegradable Mg−Zn−Ca alloy, J. Magnes. Alloy. 9 (2021) 1578–1594. https://doi.org/10.1016/j.jma.2020.08.017.

[61] M. Popa, L.M. Stefan, A.-M. Prelipcean, S.I. Drob, M. Anastasescu, J.M. Calderon Moreno, Inhibition of Mg corrosion in physiological fluids by carbonate coating, Corros. Sci. 209 (2022) 110775. https://doi.org/10.1016/j.corsci.2022.110775.

[62] Y.H. Ho, K. Man, S.S. Joshi, M. V. Pantawane, T.C. Wu, Y. Yang, N.B. Dahotre, In-vitro biomineralization and biocompatibility of friction stir additively manufactured AZ31B magnesium alloy-hydroxyapatite composites, Bioact. Mater. 5 (2020) 891–901. https://doi.org/10.1016/j.bioactmat.2020.06.009.

[63] A.I. Klyndyuk, M. Mosiałek, D.S. Kharitonov, E.A. Chizhova, M. Zimowska, R.P. Socha, A. Komenda, Structural and electrochemical characterization of YBa(Fe,Co,Cu)2O5+δ layered perovskites as cathode materials for solid oxide fuel cells, Int. J. Hydrogen Energy. 46 (2021) 16977–16988. https://doi.org/10.1016/j.ijhydene.2021.01.141.

[64] C.H. Shih, C.Y. Huang, T.H. Hsiao, C.S. Lin, The effect of the secondary phases on the corrosion of AZ31B and WE43-T5 Mg alloys, Corros. Sci. 211 (2023) 110920. https://doi.org/10.1016/j.corsci.2022.110920.

[65] Z. Chen, H. Li, X. Liang, M.-C. Zhao, K. Zhang, A. Atrens, In-situ observation on filiform corrosion propagation and its dependence on Zr distribution in Mg alloy WE43, J. Magnes. Alloy. (2022). https://doi.org/10.1016/j.jma.2022.09.033.

[66] V. Shkirskiy, P. Keil, H. Hintze-Bruening, F. Leroux, T. Stimpfling, D. Dragoe, K. Ogle, P. Volovitch, MoO<inf>4</inf>$^{2-}$ as a soluble inhibitor for Zn in neutral and alkaline solutions, Corros. Sci. 99 (2015) 31–41. https://doi.org/10.1016/j.corsci.2015.05.005.

[67] K.C. Emregül, A.A. Aksüt, The effect of sodium molybdate on the pitting corrosion of aluminum, Corros. Sci. 45 (2003) 2415–2433. https://doi.org/10.1016/S0010-938X(03)00097-0.